Eur. Phys. J. Special Topics **205**, 167-182 (2012)

DOI: 10.1140/epjst/e2012-01569-3

THE EUROPEAN PHYSICAL JOURNAL SPECIAL TOPICS

Review

Black swans, power laws, and dragon-kings: Earthquakes, volcanic eruptions, landslides, wildfires, floods, and SOC models

M.K. Sachs[1], M.R. Yoder[1], D.L. Turcotte[2], J.B. Rundle[1,2,3], and B.D. Malamud[4]

[1] Department of Physics, University of California, Davis, CA 95616, USA
[2] Department of Geology, University of California, Davis, CA 95616, USA
[3] Santa Fe Institute, Santa Fe, NM 87185, USA
[4] Department of Geography, Kings College London, London WC2R2LS, UK

Received 23 November 2011 / Received in final form 09 March 2012
Published online 01 May 2012

Abstract. Extreme events that change global society have been characterized as black swans. The frequency-size distributions of many natural phenomena are often well approximated by power-law (fractal) distributions. An important question is whether the probability of extreme events can be estimated by extrapolating the power-law distributions. Events that exceed these extrapolations have been characterized as dragon-kings. In this paper we consider extreme events for earthquakes, volcanic eruptions, wildfires, landslides and floods. We also consider the extreme event behavior of three models that exhibit self-organized criticality (SOC): the slider-block, forest-fire, and sand-pile models. Since extrapolations using power-laws are widely used in probabilistic hazard assessment, the occurrence of dragon-king events have important practical implications.

1 Introduction

The statistics of extreme events have been studied extensively [1]. Applications include floods, wars, financial crashes, and many others. Extreme events that change global society were characterized as black swans by Taleb [2]. The frequency-size distributions associated with many natural hazards satisfy power-law (fractal) statistics to a good approximation [3]. Examples include earthquakes, landslides, volcanic eruptions and wildfires. We will argue that floods also fit into this category. An important question in probabilistic hazard assessment is whether future extreme events can be forecast by extrapolating the power-law behavior.

In some cases small events satisfy power-law scaling but one or more extreme events are significantly larger than the extrapolation of the power-law scaling. Sornette [4] refers to this class of extreme events as dragon-kings. Examples of dragon-kings would be the population of London and Paris relative to the power-law distribution of the population of the other cities in the U.K. and France. Another example of dragon-king behavior is material fracture. When stress on a brittle material

is increased there is often a power-law distribution of acoustic emissions before an unstable fracture propagates through the sample [5]. The precursory emissions are a nucleation process and the fracture can be classified as a phase change [6].

In this paper we will address the question: Are dragon-kings relevant to probabilistic hazard assessment? Our discussion will emphasize seismic hazard. On relatively large geographic scales the frequency-rupture-area statistics of earthquakes are well represented by power-law statistics even for the largest events. However, this behavior does not seem to be the case locally. On major faults, such as the San Andreas in California, seismic activity is dominated by great earthquakes, like the 1906 San Francisco earthquake. These are known as "characteristic" earthquakes and we will argue that characteristic earthquakes are dragon-kings. As a specific example we will consider a characteristic earthquake cycle on the Parkfield segment of the San Andreas fault. We will then consider in some detail the use of slider-block models to represent seismicity. We will show that dragon-king behavior can be generated by these models.

We will then extend our studies to volcanic eruptions, landslides, and wildfires. These exhibit power-law scaling and we will discuss their extrapolation to the largest events. The statistics of extreme floods have been the subject of many studies. We will discuss the extrapolation of small flood observations to large floods in some detail.

2 Global seismicity

The frequency-magnitude statistics of earthquakes have been recognized to satisfy log-linear scaling both globally and regionally. It is accepted that earthquakes satisfy the Gutenberg-Richter (GR) scaling relation [7]

$$\log N_c = -bm + a, \tag{1}$$

where N_c is the cumulative number of earthquakes in a region and time interval with magnitudes greater than m. The scaling relation given in Eq. 1 has been shown to be equivalent to a power-law scaling between N and A_r, the earthquake rupture area [3].

$$N_c = \alpha A_r^{-b}. \tag{2}$$

Thus earthquakes satisfy power-law scaling. Great earthquakes will be dragon-kings if their magnitudes exceed significantly the extrapolated scaling relation given in Eq. 2.

In this section we will consider global seismicity. Because of the many problems associated with the magnitudes of large earthquakes, the preferred approach to global seismicity is to use the Global Central Moment Tensor catalog (www.globalcmt.org) [8,9]. We utilize this catalog for the period January 1, 1977 to September 30, 2010. In order to update our results through August 15, 2011 we use moment magnitudes given in the ANSS catalog (`www.ncedc.org/cnss/`). Using these catalogs the cumulative number of global earthquakes with magnitudes greater than m for the period 1977 to August 15, 2011 is given in Fig. 1. The roll over for small magnitudes $m_w < 5.25$ is attributed to the sensitivity limit of the global network used to obtain moment magnitudes m_w [10]. The roll over for $m_w > 7.5$ is more controversial [11,12]. It is usually attributed to the transition from small earthquakes with near equal lengths and depths to large earthquakes with lengths much larger than depths.

Included in Fig. 1 is the least squares fit of Eq. (1) to the data taking $a = 9.643$ and $b = 0.996$. The fit is carried out between $m = 5.6$ and 7.5 and includes some 30,000 earthquakes. Also included in Fig. 1 are the $m_w = 9.0$ Sumatra earthquake on December 26, 2004 and the $m_w = 9.1$ Tohuko (Japan) earthquake on March 11, 2011.

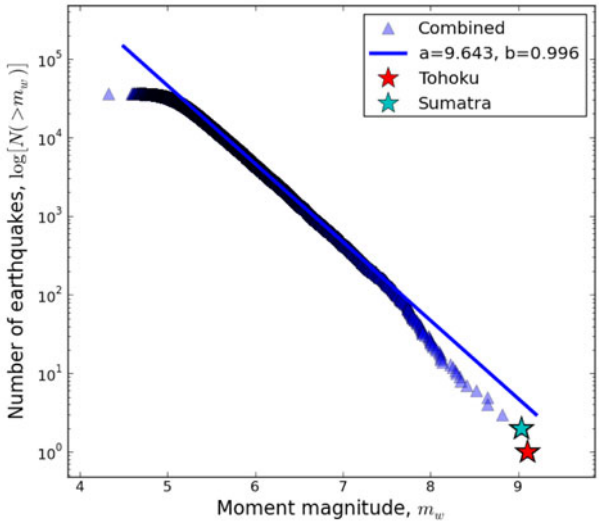

Fig. 1. Cumulative number of global earthquakes N with magnitude greater than m_w are given as a function of moment magnitudes m_w. Observed values for the period January 1, 1977 to September 30, 2010 are obtained from the global CMT catalog, values for the period October 1, 2010 to August 15, 2011 are obtained from the ANSS catalog. The least-squares best fit of Eq. (1) to the values in the range $5.5 \leq m_w \leq 7.5$ is given taking $a = 9.643$ and $b = 0.996$. Also included are the 2004 $m_w = 9.0$ Sumatra earthquake and the 2011 $m_w = 9.1$ Tohuko earthquake.

These were the largest earthquakes during the study period. The tsunami generated by the Sumatra earthquake killed some 230,000 people. The earthquake and tsunami generated by the Tohuko earthquake killed some 22,000 people. In addition the tsunami resulted in a nuclear meltdown at the Fukushima I power plant. This meltdown created serious economic disruption in Japan and threatens to curtail the global use of nuclear power plants to reduce the emission of greenhouse gasses. The size and impact of the Sumatra and Tohuko earthquakes clearly qualify them as black swans. However, since they lie below the extrapolation of the power-law scaling they are not dragon-kings on a global scale. We will argue in the next section that earthquakes do exhibit dragon-king behavior on a regional scale.

3 Characteristic earthquakes

There are two limiting hypotheses for the behavior of faults. In the first, each fault (or fault segment) has a sequence of earthquakes that rupture the entire fault (or fault segment). The global GR (power-law, fractal) distribution of earthquakes illustrated in Fig. 1 is attributed to a power-law (fractal) distribution of fault areas. Each fault has an earthquake with rupture area equal to the area of the fault. In seismology these are known as "characteristic" earthquakes. The other limiting hypothesis is that every fault has a GR distribution of earthquake magnitudes. The global GR scaling is the sum of the GR scaling on individual faults. The actual behavior of the earth lies between these two limits [13].

Ideally, observations would discriminate between the two limiting hypotheses. However, it is impossible to attribute smaller earthquakes to specific faults because only the largest faults can be mapped and identified. Also, location errors of smaller

earthquakes make their association with each other and individual faults very difficult. The generally accepted view in seismology is that smaller earthquakes on a fault obey power-law (GR) scaling but a large fraction of the deformation on the fault is associated with large quasi-periodic "characteristic" earthquakes. Thus these large "characteristic" earthquakes satisfy the condition to be dragon-kings. In a paper entitled "The Gutenberg-Richter or characteristic earthquake distribution, which is it?", Wesnousky [13] has given data to support the generally accepted view that a working definition of characteristic earthquakes is that they are large earthquakes on plate-boundary faults. As examples we consider two major plate-boundary faults: (1) The San Andreas fault in California is a major boundary fault between the Pacific and North American plates and (2) the subduction zone fault (unnamed) above the Pacific plate as it is being subducted beneath Japan.

A comprehensive study of characteristic earthquakes has been carried out on the southern section of the San Andreas fault. Paleoseismic studies using radiocarbon dating of fluidized sediments at the Wrightwood site [14] date characteristic earthquakes at (in years CE): 534 (407-628), 634 (551-681), 697 (657-722), 722 (695-740), 781 (736-811), 850 (800-881), 1016 (957-1056), 1116 (1047-1181), 1263 (1191-1305), 1487 (1448-1518), 1536 (1508-1569), 1685 (1647-1717), 1812 (historic), 1857 (historic). The ranges of values are the 95% confidence intervals on the radiocarbon dates. The 1857 earthquake was an historic earthquake that ruptured some 400 km of the fault from centeral California to the Los Angeles area. No seismic recordings were available at the time of this earthquake but measurements of surface displacements indicate a magnitude $m \approx 8.2$. In the past 75 years no earthquake with $m > 5.5$ has occurred on this fault segment. If GR scaling were valid for this fault $m > 5.5$ earthquakes would be expected every year. For GR scaling to be valid there should be 100 $m > 6$ earthquakes for each $m = 8$ earthquake. Seismologists generally accept that the sequence of paleo-earthquakes listed above are characteristic earthquakes [13]. Similarly the 1906 earthquake that destroyed San Francisco is generally accepted to be a characteristic earthquake on the northern San Andreas fault. However, paleoseismic sites are not available on the rupture zone of this earthquake.

Similar paleoseismic studies have dated characteristic earthquakes on the southern Nankai Trough segment of the subduction zone beneath Japan. Characteristic earthquakes occurred in 684, 887, 1099, 1361, 1605, 1707, 1854, and 1946. The dates for these earthquakes were obtained using a variety of historic and other records [15]. The Tohuko earthquake was a characteristic earthquake on the northern section of this fault and is similar to the San Francisco earthquake in that paleoseismic data are not available [13].

The best documented sequence of characteristic earthquakes occurred on the Parkfield segment of the San Andreas fault in California. Evidence suggests that earthquakes with $m \approx 6$ occurred in 1857, 1881, 1901, 1922, 1934, 1966, and 2004 [16]. Based on seismograms the 1922, 1934, 1966, and 2004 events were remarkably similar in magnitude. The Parkfield earthquakes are globally unique in that they are a sequence of relatively small plate- boundary "characteristic" earthquakes. Thus they occur frequently and a complete "characteristic" earthquake cycle can be studied. In order to study the seismicity associated with the 2004 "characteristic" earthquake we consider earthquakes during the period 1972 (five years after the $m = 6.0$, June, 1966 earthquake) to 2009 (five years after the $m = 5.95$, 28 September, 2004 earthquake). To isolate seismicity associated with the characteristic Parkfield earthquake we confine our study to the region where aftershocks of the 2004 earthquake were concentrated [17].

The region is elliptical, centered at 35.9° N and −120.5° W with semi-major and semi-minor axes of 0.4° and 0.15° respectively, oriented at 137° NW. Both the aftershocks and the elliptical region are shown in Fig. 2. It is standard practice to

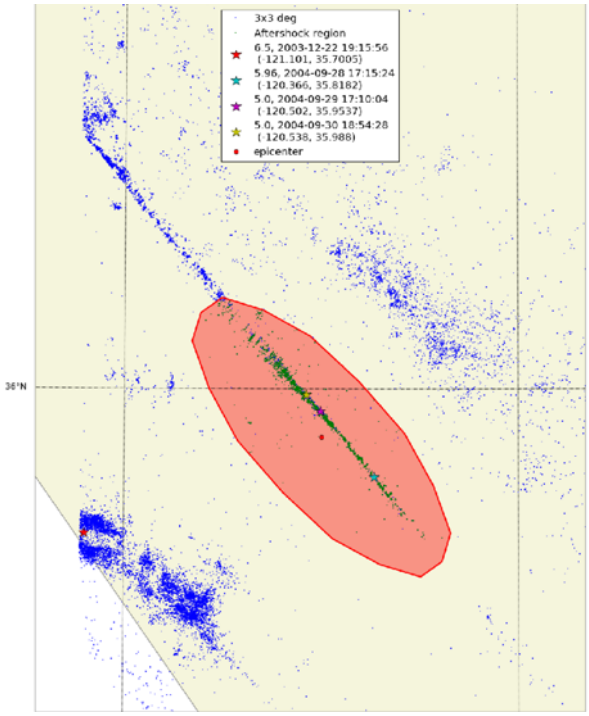

Fig. 2. Seismicity in central California for the period 28 September, 1999 to 28 September 2009. The aftershocks of the 18 September, 2004 Parkfield earthquake are shown in the red elliptical area. Aftershocks of the 2004 San Simean earthquake and residual aftershocks of the 1983 Coalinga earthquake are clearly seen to the south-west and north-east of the study region.

associate the aftershock regions with correlated seismicity to study a characteristic earthquake [13,18,19]. Another advantage of the Parkfield region is the localization of the correlated seismicity. This region clearly excludes the aftershocks of the $m = 6.5$ (2004) San Simean earthquake (lower left hand corner in Fig. 2) and the aftershocks of the $m = 6.5$ (1983) Coalinga earthquake (just above the red elliptical area).

Parkfield is the site of the highest quality local seismic network in the world [16]. This network was constructed by the U.S. Geological Survey in the 1980's in the expectation that the next characteristic earthquake would occur. In our analysis we have used the catalog provided by the Northern California Earthquake Data Center (NCSN catalog, `quake.geo.berkeley.edu/ncedc/`).

The cumulative frequency-magnitude distribution of earthquakes in the Parkfield aftershock region for the period 1972 to 2009 is given in Fig. 3. The best-fit scaling to this distribution is given by

$$N = 4.47 \times 10^5 10^{-m}. \tag{3}$$

This is the least-squares best fit to the data in the range $2.5 < m < 4.5$. Over this range there are some 3,000 data points. The roll over for $m < 2.5$ is attributed to a lack of sensitivity of the network for small magnitudes [17]. The roll over for $m > 4.5$ is attributed to the relatively small number of earthquakes: $N \simeq 10$ [17]. If this scaling was applicable to the characteristic earthquake ($N = 1$) it's magnitude would have been $m = 5.65$. The $m = 5.95$ Parkfield main shock clearly lies above the extrapolation of the power-law correlation of the smaller earthquakes. An important question

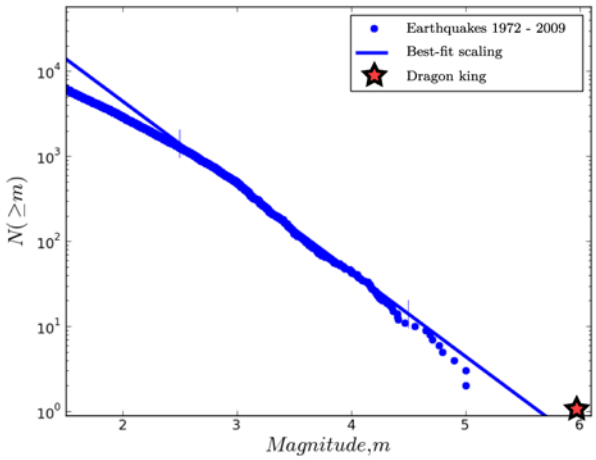

Fig. 3. Cumulative number of earthquakes with magnitude greater than m as a function of m for the Parkfield earthquake cycle 1972 to 2009. The best-fit scaling from Eq. (3) is also shown. The $m = 5.95$ Parkfield earthquake is shown as a dragon-king.

is whether the difference between $m = 5.65$ and $m = 5.95$ can be attributed to the statistical variability of the characteristic earthquakes. Excellent seismic records are available for the 1934, 1966, and 2004 characteristic earthquakes. The magnitudes are $m = 6.0 \pm 0.1$. In addition the seismic records of the 1934 and 1966 earthquakes are essentially identical indicating near identical points of rupture initiation and propagation pattern. The 2004 earthquake has a somewhat different rupture pattern but the rupture zone is considered to very nearly identical to the earlier earthquakes. The evidence is that these are truly characteristic earthquakes that rupture the same specified segment of the San Andreas fault. The possibility that one of these characteristic earthquakes could have had a magnitude as low as 5.65 is excluded by the available data. Thus we conclude that the sequence of characteristic earthquakes of the Parkfield segment are dragon-kings. Although the $\Delta m = 0.3$ difference between the 2004 Parkfield event and what one would expect from extrapolating the scaling relation in Eq. (3) may not seem large, it represents about a factor of three difference in energies which does set it above the extrapolated GR background.

For reasons stated above the Parkfield characteristic earthquake cycle is the only such cycle that can be studied in detail using a high quality earthquake catalog. However, based on the absence of earthquakes adjacent to other segments of the San Andreas fault and other faults where characteristic earthquakes occur, we conclude that characteristic earthquakes are dragon-kings with respect to the correlated seismicity (including aftershocks). The background seismicity satisfies power-law Gutenberg-Richter statistics but the characteristic earthquakes lie above the extrapolation as shown in Fig. 3.

4 Slider-block model

The multiple slider-block model has been proposed as a deterministic example of self-organized critical behavior [20]. This model had previously been proposed as a simple model of earthquake behavior [21]. Utilizing the multiple slider-block simulations of Abaimov et al. [22] we will demonstrate dragon-king behavior.

A linear chain of 100 slider blocks was pulled over a surface at a constant velocity by a loader plate as illustrated in Fig. 4. Each block is connected to the loader plate

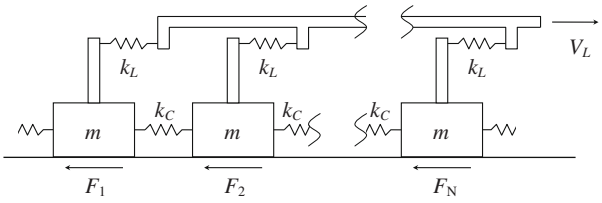

Fig. 4. Illustration of the one-dimensional slider-block model. A linear array of N blocks of mass m are pulled along a surface by a constant velocity V_L loader plate. The loader plate is connected to each block with a loader spring with spring constant k_L and adjacent blocks are connected by springs with spring constant k_C. The frictional resisting forces are $F_1, F_2, \ldots, F_N$.

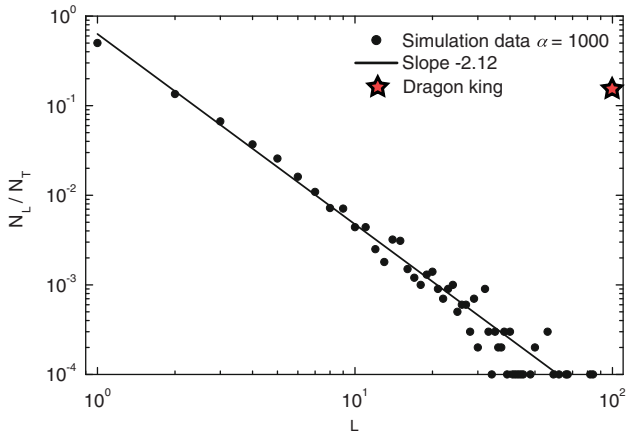

Fig. 5. Frequency-size distribution of 10,000 slip events for a "stiff" system with $\alpha = 1000$. The ratio of the number of events N_L of event size L to the total number of events N_T is given as a function of L. The solid line is a power-law dependence with exponent -2.12. System-wide ($L = 10^2$) dragon-king events are clearly illustrated.

by a spring with spring constant k_L and adjacent blocks are connected to each other by springs with spring constant k_C. An important parameter in the problem is the ratio of spring constants $\alpha = k_C/k_L$. This is a measure of the stiffness of the system. The blocks interact with the surface through a static-dynamic friction law. With the static coefficient of friction larger than the dynamic (sliding) coefficient of friction, stick-slip behavior is observed. The size of a slip event is given by the number of blocks L that slip simultaneously in the event.

The stiffness α acts as a tuning parameter in this problem. For soft systems (small α) only small slip events occur, there is an exponential decay for larger slip events. As α is increased system wide ($L = 100$) events begin to occur. The frequency-size distribution of the slip events for a stiff system ($\alpha = 1000$) is given in Fig. 5. Statistics for 10,000 events are given and about 1,500 are system wide ($L = 100$) events. The small events are well approximated by the power-law relation

$$\frac{N_L}{N_T} = 0.8L^{-2.12}, \tag{4}$$

where N_L is the number of events with L blocks slipping and $N_T = 10,000$ is the total number of events. However, the large number of system wide events ($L = 100$) do not scale with the smaller events. The results are clearly an example of dragon-king

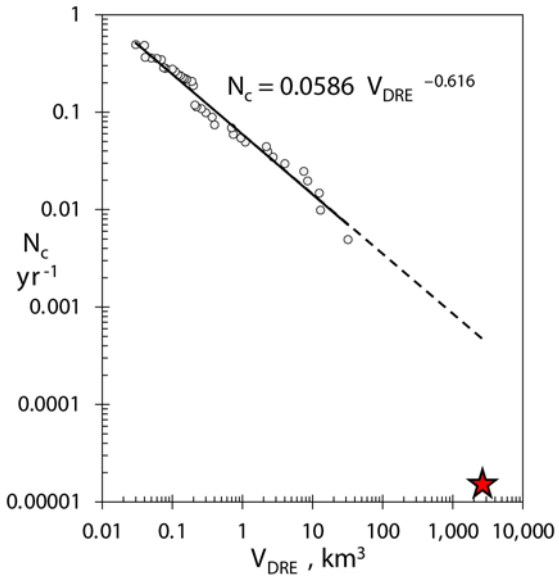

Fig. 6. Cumulative number of volcanic eruptions N_c during the period 1800-2002 with dense rock equivalent volume greater than V_{DRE} as a function of V_{DRE}. The best-fit power-law scaling from Eq. (5) is also shown along with the Toba eruption (red star).

behavior. The occurrence of the dragon-kings is determined by the size of the system. They are not a finite-size effect in that they do not disappear as the system becomes very large. This behavior has been discussed for earthquakes and other systems [23,24] and for epileptic seizures [25]. The system wide events are quite analogous to the characteristic earthquakes on a fault, again an effect related to system size.

5 Volcanic eruptions

Volcanic eruptions are quantified in terms of the dense rock equivalent volume V_{DRE}. This is the volume of magma ejected as tephra (pumice and ash) during an explosive eruption and/or the volume of lava extruded.

In April 1815 an eruption on Mount Tambora in Indonesia resulted in the generation of about $V_{DRE} = 32\,\mathrm{km}^3$ of ash [26]. This ash and associated gases resulted in global cooling, 1816 was known as the year without a summer. In the northeastern United States snow or frost occurred in every month of the year and a global famine resulted. Certainly this event could be called a black swan.

The frequency-volume distribution of major eruptions is given in Fig. 6 for the period 1800 to 2002. The cumulative number per year N_C is given as a function of dense rock equivalent volume V_{DRE} [27]. It is seen that this data are well approximated by the power-law (fractal) relation

$$N_c = 0.0586 V_{DRE}^{-0.616}, \tag{5}$$

with V_{DRE} in km^3. The Tambora eruption with $V_{DRE} = 32\ \mathrm{km}^3$ was the largest eruption since 1800 but does not deviate significantly from the power-law scaling. Thus while the eruption was certainly a black swan in terms of global impact it was not a dragon-king in terms of being unexpected.

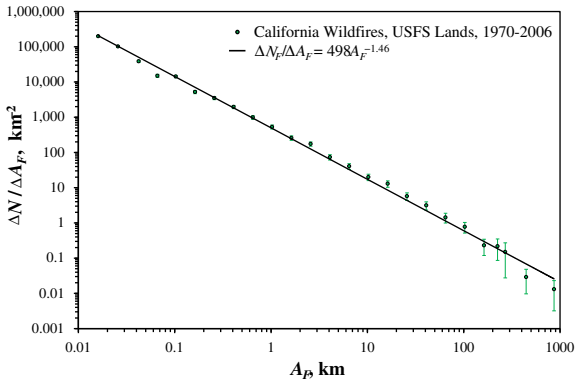

Fig. 7. Frequency-area statistics for 7,422 wildfires on United States Forest Service lands in California for the period 1970–2006 [33]. The frequency densities $\Delta N_F/\Delta A_F$ are given as a function of burned area A_F. Also shown is the best least-square power-law fit to the data.

From Fig. 6 we see that the power law frequency-volume relation for volcanic eruptions is a good approximation in the range $0.04 < V_{DRE} < 10\,\mathrm{km}^3$. An important question is whether this scaling can be extrapolated to longer time frames, i.e. the dashed line in Fig. 6. Certainly, just as in the case of earthquakes the power-law scaling must roll over for very large events. An eruption cannot be larger than the size of the earth.

Another catastrophic eruption at Lake Toba, Sumatra is estimated to have erupted $V_{DRE} = 2,750 \pm 250\,\mathrm{km}^3$ of dense rock equivalent $73,500 \pm 500$ years ago [28]. There is evidence that this eruption had a strong impact on human evolution [29] and could certainly be called a black swan. Taking $V_{DRE} = 2,750\,\mathrm{km}^3$ and assuming that this is an eruption that would occur only once in 73,500 years, i.e. $N_c = 73,500^{-1}\,\mathrm{yr}^{-1} = 1.36 \times 10^{-5}\,\mathrm{yr}^{-1}$ we also show this eruption in Fig. 6. From Eq. (5) the largest eruption expected in 73,500 years ($N_c = 1.36 \times 10^{-5}\,\mathrm{yr}^{-1}$) would have volume $V_{DRE} = 7.9 \times 10^6\,\mathrm{km}^3$. This is a 200 km cube of rock. Such an eruption is clearly impossible so that power-law scaling must roll over on a time scale considerably less than 75,000 years. We conclude that although the Lake Toba eruption was certainly a black swan, the eruption was not unexpected in terms of the power-law scaling given in Eq. (5) and cannot be considered a dragon-king. We would suggest an exponential roll over in Fig. 6 for volumes greater then $V_{DRE} \approx 10^2\,\mathrm{km}^3$. Volcanoes capable of producing dens rock equivalent eruptions with volumes greater than $1,000\,\mathrm{km}^3$ are known as supervolcanoes. In addition to Lake Toba, other supervolcanoes are Taupo, New Zealand and Yellowstone, U.S.A.

An interesting question is whether characteristic eruptions occur on individual volcanoes in analogy to characteristic earthquakes on faults. Also whether smaller eruptions on a volcano satisfy power-law frequency-magnitude statistics. Unfortunately there are not sufficient data available to answer these questions.

6 Wildfires

Many studies have been carried out on the frequency-area statistics of wildfires [30–32]. The general consensus is that they are well approximated by power-law distributions. As an example we give the frequency-area statistics for 7,422 wildfires in

California in Fig. 7. These fires were on United States Forest Service lands during the period 1970 to 2006 [33]. The frequency densities of fires $\Delta N_F/\Delta A_F$ are given as a function of burned areas A_F. Also included is the best fit power-law distribution given by

$$\frac{dN_F}{dA_F} = 498 A_F^{-1.48}, \tag{6}$$

with A_F in km^2. An excellent power-law scaling is seen. There is no evidence for anomalously large fires, i.e. dragon-kings, in the data set and in the many other power-law correlations that have been published (i.e. [29–31]).

Fire suppression appears to increase the occurrence of large fires. Minnich [34,35] studied this effect by comparing the frequency-area distribution of wildfires in southern California, where anthropogenic fire suppression was extensive, with distributions in Baja California, where suppression is uncommon. Both distributions were in reasonably good agreement with power laws but with a larger slope (fewer large fires) in Baja California. This analysis is consistent with studies of fire return intervals (FRI) and fire intensities in the Klamath Natioal Forest area [36–38], particularly in conjunction with numerical modeling [39]. Collectively, these studies indicate that fire suppression changes the exponent in the power-law correlations but does not lead to large dragon-king fires.

7 Forest-fire model

The power-law scaling of wildfires is associated with the behavior of the forest-fire model [30]. The standard forest-fire model [40] consists of a square grid of sites. At each time step either a model tree or match is dropped on a randomly chosen site. A tree is "planted" only if the site is unoccupied. If a match is dropped on an occupied site, that tree and all adjacent trees "burn" and are removed from the grid. The governing parameter in this model is the firing frequency f_s: the fraction of time steps in which matches are dropped. If $f_s = 1/125$ there have been 124 attempts to plant trees before a match is dropped on the 125th time step. After specifying the size of the square grid N_G and the firing frequency f_s a simulation is run for N_S time steps. The number of trees that burn in model fires is determined. Taking $N_G = 16,384$ (128×128), $f_s = 1/125$, $1/500$, and $1/2000$ and $N_S = 10^9$ we plot the fraction of time steps on which fires of area A_F occur: N_F/N_S, against A_F in Fig. 8.

The behavior of this model is very similar to the behavior of the slider-block model described above. The roles of the stiffness parameter α in the slider-block model and the firing frequency in the forest fire model are virtually identical. For large firing frequencies only small fires occur, there is an exponential decay for larger fires. As f_s is decreased fires begin to span the grid. They are an effect associated with the size of the grid of planting sites. For very small firing frequencies this behavior occurs in the forest-fire model just as in the slider-block model illustrated in Fig. 5. In the limit of a near zero firing frequency all fires will burn all sites on the grid.

It is interesting to note that the data represented in Fig. 7 shows evidence of neither roll over (high firing frequency) nor system size effects (low firing frequency) for fires in California. It is unclear at this time to what extent this is evidence of a dynamic effective firing frequency f_s, presumably related to regional fuel density and fire susceptibility in general, or simply an incomplete historical record. Frequency-area distributions of wildfires in Canada do, in fact, demonstrate large area truncation [41].

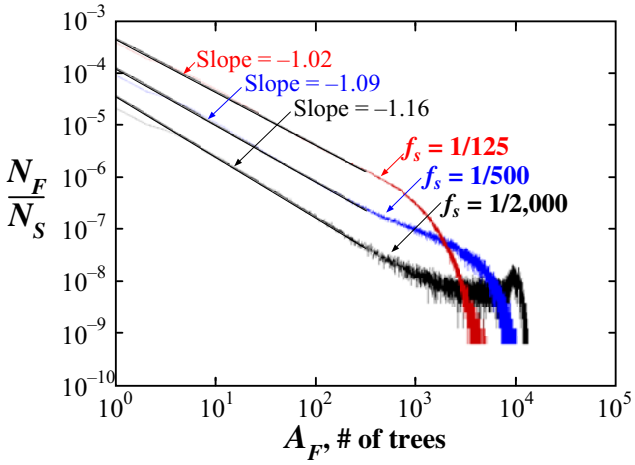

Fig. 8. Noncumulative frequency-area distributions for the forest-fire model [30]. The number of fires N_F with area A_F is given. Results are given for sparking frequencies $f_s = 1/125$, 1/500, 1/2000.

8 Landslides

Relatively few inventories of landslide frequency-area distributions are available. One reason is that landslide scars are subject to relatively rapid erosion. A number of triggered landslide events have been analyzed while still fresh. Three examples [42] are given in Fig. 9. These are:

1. 11,111 landslides triggered by the 17 January 1994 Northridge, California earthquake.
2. 4,237 landslides triggered by a snowmelt event in the Umbria region of central Italy in January 1997.
3. 9,594 landslides triggered by heavy rains from Hurricane Mitch in Guatemala in late October and early November 1998.

The probability densities p of the distributions are given as a function of landslide area A_L in Fig. 9. Also shown in Fig. 9 is the least-squares best-fit gamma distribution. For large landslides ($A_L > 200\,\mathrm{m}^2$) this best-fit distribution reduces to the power-law correlation

$$p(A_L) = 10^{-4} A_L^{-2.4}, \tag{7}$$

with A_L in km^2.

The frequency-area distributions for the larger landslides generally satisfy power-law correlations to a good approximation [42]. There is no evidence for anomalously large dragon-king landslides in these distributions. Certianly many large landslides have been documented and some of these could be dragon-kings. However, relevant inventories are not available so a statistical study such as illustrated in Fig. 9 cannot be carried out. It is also relevant to note that rock falls must be considered separately as their statistics are different than landslides [42].

9 Sandpile model

The concept of self-organized criticality was originally based on the "sandpile" model proposed by Bak et al. [43]. In this model there is a square grid of boxes. At each

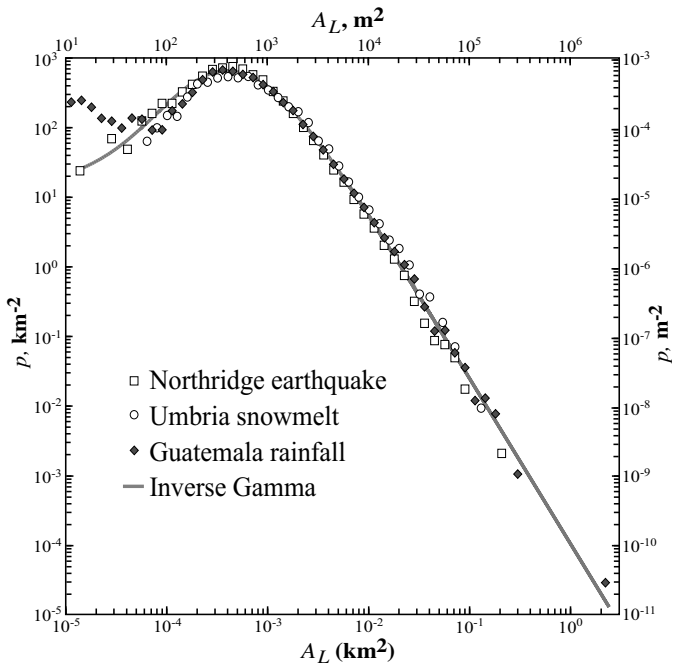

Fig. 9. Frequency-area statistics for three landslide inventories [42]: (1) 11,111 landslides triggered by the Northridge earthquake, (2) 4,237 landslides triggered by a snowmelt event Italy, (3) 9594 landslides triggered by Hurricane Mitch. The probability density p is given as a function of landslide area A_L. Also shown is the least-squares best-fit gamma distribution.

time step a particle is dropped into a randomly selected box. When a box accumulates four particles they are redistributed to the four adjacent boxes, or in the case of edge boxes, are lost from the grid. These redistributions can lead to further instabilities and "avalanches" of particles are lost from the grid. A measure of the size of a model avalanche is the number of boxes (area) A_L that participate in an avalanche. The noncumulative frequency-area distribution of avalanches for a simulation on a 50×50 grid is given in Fig. 10. Good agreement with a power-law distribution is obtained with an exponent of 1.03.

The behavior of the sandpile model illustrated in Fig. 10 is quite different than the behavior of the slider-block and forest-fire models in Figs. 5 and 8. The sandpile model does not have a tuning parameter. All three models exhibit power-law scaling with exponents near unity and thus all three are referred to as examples of self-organized criticality. However, the sandpile model, unlike the others, does not exhibit dragon-king behavior. This difference can be attributed to the lack of a tuning parameter. In the sandpile model the power-law behavior extends to the size of the grid. However, in the slider-block and forest-fire models the range of power-law behavior is a function of the value of the control parameter.

10 Floods

Floods are a major hazard to many cities and estimates of flood risk have serious economic consequence. Floods are quantified in terms of the volumetric discharge at a point on a river. The discharge $Q(T)$ is the maximum discharge associated with a recurrence interval of T years, that is $Q(100)$ is the maximum flow expected once

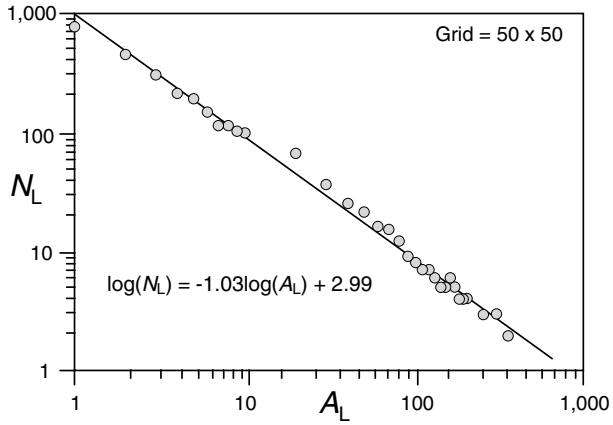

Fig. 10. Noncumulative frequency-area distribution of avalanches for the sandpile model. The number of avalanches N_L with area (number of boxes) A_L is given. The best-fit power-law correlation is given.

every 100 years, i.e. the 100 year flood. Flood-frequency estimates are empirical and a wide variety of statistical distributions have been used [44]. Record floods can cause large loss of life, property damage, and crop damage. Thus record floods can be classified as black swans. Record floods appear to occur more often than predicted by flood frequency estimates. Thus they may be dragon-kings.

In our discussion we will focus our attention on floods that have occurred on the Colorado River [45], in particular on paleo-floods that occurred up to 1,400 years ago. We first consider discharge obtained at the Lees Ferry gauge during the period 1921–1962 (more recent observations were influenced by the construction of the Glen Canyon Dam). Federally mandated flood frequency forecasts in the United States utilize the sequence of maximum annual floods at a gauging station. This flood is the peak discharge $Q(1)$ during a water year: October 1 of the previous year to September 30 of the year in question. The yearly floods are ranked from largest to smallest. For the 42 year record at the Lees Ferry gauge the largest flood is given a period $T = 42$ years, the second largest flood a period of $T = 21$ years, and so forth to the smallest annual flood with a period of $T = 1$ year. These values are given in Fig. 11.

The federally mandated forecasts utilize the log Pearson type 3 (LP3) distribution to fit the annual values. This distribution is then extrapolated to forecast future floods. This mandated forecast is also illustrated in Fig. 11.

A major problem with the annual flood series is that several statistically independent floods in a water year may be larger than the annual flood in another water year. To overcome this difficulty the partial duration flood series was introduced [45]. In this flood series a peak flow must be separated by at least 30 days to be defined as an independent flood. For the 42 year Colorado River sequence the largest 42 independent peak flow are taken to be the partial duration flood series. The partial duration flood series for the Lees Ferry gauge data is also shown in Fig. 11. The two flood series strongly diverge for periods less than five years and for future extrapolations.

The LP3 distribution is a relatively thin-tailed distribution. The applicability of the fat-tailed power-law distribution to floods has been suggested [46]. In this case we have

$$Q(T) = CT^{\alpha}. \tag{8}$$

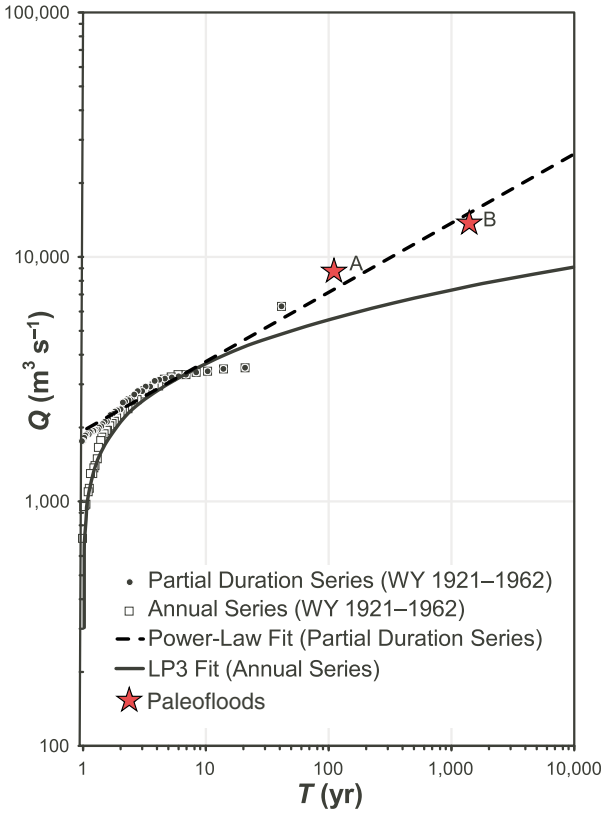

Fig. 11. Dependance of the maximum daily discharge Q associated with time period T for the Colorado River in the Grand Canyon, Arizona [46]. The annual and partial duration flood series at the Lees Ferry gauging station for the water years 1921–1962 are shown. The least-squares power-law fit to the partial duration series and the LP3 fit to the annual series are also given. Points A and B are estimates of two paleo-floods [47].

Instead of using the annual floods for analysis, the partial-duration flood series is used. The best fit of Eq. 8 to the Lees Ferry data requires $C = 3.28$ and $\alpha = 0.28$, this fit is illustrated in Fig. 11.

Two paleo-flood discharge estimates on this section of the Colorado River were obtained by O'Connor et al. [47]. The levels of flood debris were used to estimate discharge and radiocarbon dates on the debris were obtained. The results are shown as points A and B in Fig. 11. Point A is interpreted as the historic Colorado River flood of 1884. The discharge is estimated to be $Q = 8,800\,\mathrm{m^3\,s^{-1}}$ and it is assigned a recurrence interval of $T = 112$ years. Point B is estimated to have had a discharge $Q = 14,000\,\mathrm{m^3\,s^{-1}}$ with an age 1200–1600 years BP, it is assigned a recurrence interval $T = 1400$ years. While the paleo-floods exceed the LP3 fit by a considerable amount, they are quite close to the power-law fit. Since the definition of a dragon-king implies the extrapolation of power law scaling, we conclude that the two paleo-floods were not dragon-kings. While we have only given one example, other studies [46] indicate extreme floods are well estimated by the power-law scaling as defined in Eq. (8).

11 Discussion

The clearest example of dragon-king behavior given in this paper is the stiff slider-block model illustrated in Fig. 5. The small slip events satisfy power-law (fractal)

statistics, but an anomalously large number of system-wide events occur. There are two scaling parameters in the slider-block model, the stiffness of the system $\alpha = k_C/k_L$ and the size of the system L. With fixed L, the range of power-law behavior increases with increasing stiffness. When this range extends to the system size L, system wide events occur. The larger the system size L, the larger the stiffness parameter α required to get system wide events. Very stiff systems exhibit well defined dragon-king behavior. We have also shown that the forest-fire model exhibits dragon-king behavior as illustrated in Fig. 8. The extrapolation is identical to that of the slider-block model with the firing frequency f_s playing the role of the stiffness. However, as shown in Fig. 10, the sandpile model does not have anomalously-large system-wide events. This is because there is no tuning parameter in this model.

In terms of the natural phenomena considered in this paper, characteristic earthquakes on faults can be associated with dragon-king behavior. We have illustrated this with the characteristic earthquake on the Parkfield segment of the San Andreas fault. The smaller earthquakes on and adjacent to the fault satisfy power-law statistics but the magnitude of the characteristic earthquake lies above the extrapolation of the power-law behavior as illustrated in Fig. 3. This behavior is generally accepted by seismologists [13]. This led to the concept of characteristic earthquakes: the large set of quasi-periodic earthquakes that occur on recognized faults.

We have shown that global frequency-size distributions of earthquakes and volcanic eruptions exhibit power-law behavior for smaller sizes but have roll over for large events similar to the behavior of the forest-fire model for small firing frequencies. The data for wildfires, landslides, and floods are more limited and neither roll over nor dragon-king behavior has been observed.

The applicability of power-law statistics to natural hazards has important practical implications. For example, probabilistic seismic hazard studies extrapolate the rate of occurrence of small earthquakes to quantify the probability of occurrence of large earthquakes. This extrapolation would not be valid if dragon-king earthquakes occur.

This work has been funded by CRDF award #RUG1-2866-PE-07 and DOE grant #DE-FG02-04ER15568.

References

1. R.R. Kinnison, *Applied Extreme Value Statistics* (Battelle Press, Columbus, Ohio, 1985), ISBN: 0029476305
2. N. Taleb, *The Black Swan: The Impact of the Highly Improbable*, 1st edn. (Random House, New York, 2007), ISBN: 9781400063512
3. D.L. Turcotte, *Fractals and Chaos in Geology and Geophysics*, 2nd edn. (Cambridge University Press, Cambridge, UK, 1997), ISBN: 0521561647 (hardback)
4. D. Sornette, Int. Terraspace Sci. Eng. **2**, 1 (2009)
5. A. Guarino, A. Garcimartín, S. Ciliberto, Eur. Phys. J. B - Cond. Matter Complex Syst. **6**, 13 (1998)
6. M. Alava, P. Nukala, S. Zapperi, Adv. Phys. **55**, 349 (2006)
7. B. Gutenberg, C.F. Richter, *Seismicity of the Earth and Associated Phenomena* (Princeton University Press, Princeton, N.J., 1954)
8. A.M. Dziewoński, T.A. Chou, J.W. Woodhouse, J. Geophys. Res. **86**, 2825 (1981)
9. G. Ekström, A.M. Dziewoński, N.N. Maternovskaya, M. Nettles, Phys. Earth Planet. Inter. **148**, 327 (2005)

10. E.R. Engdahl, R. van der Hilst, R. Buland, Bull. Seis. Soc. Am. **88**, 722 (1998)
11. J.B. Rundle, J. Geophys. Res. **94**, 12337 (1989)
12. D. Sornette, L. Knopoff, Y. Kagen, C. Vanneste, J. Geophys. Res. **101**, 13883 (1996)
13. S.G. Wesnousky, Bull. Seismol. Soc. Amer. **84**, 1940 (1994)
14. G.P. Biasi, R.J. Weldon, T.E. Fumal, G.G. Seitz, Bull. Seis. Soc. Am. **92**, 2761 (2002)
15. M. Ando, Tectonophys. **27**, 119 (1975)
16. W.H. Bakun, B. Aagaard, B. Dost, W.L. Ellsworth, J.L. Hardebeck, R.A. Harris, C. Ji, M.J.S. Johnston, J. Langbein, J.J. Lienkaemper, et al., Nature **437**, 969 (2005)
17. R. Shcherbakov, D.L. Turcotte, J.B. Rundle, Bull. Seismol. Soc. Amer. **96**, S376 (2006)
18. R.B. Hofmann, Eng. Geol. **43**, 5 (1996)
19. T. Ishibe, K. Shimazaki, Earth Planets Space **61**, 1041 (2009)
20. J.M. Carlson, J.S. Langer, Phys. Rev. A **40**, 6470 (1989)
21. R. Burridge, L. Knopoff, Bull. Seismol. Soc. Amer. **57**, 341 (1967)
22. S. Abaimov, D. Turcotte, R. Shcherbakov, J. Rundle, G. Yakovlev, C. Goltz, W. Newman, Pure Appl. Geophys. **165**, 777 (2008)
23. D. Sornette, Images de la Physique 1993 **édition du CNRS**, 9 (CNRS, Paris, 1994)
24. D. Sornette, P. Miltenberger, C. Vanneste, *Statistical physics of fault patterns self-organized by repeated earthquakes: synchronization versus self-organized criticality*, in *Recent progress in statistical mechanics and quantum field theory. Proceedings, Conference, Los Angeles, USA, May 16–21, 1994*, edited by P. Bouwknegt, P. Fendley, J.A. Minahan, D. Nemeschansky, K. Pilch, H. Saleur, N.P. Warner (World Scientific, Singapore, 1995), p. 313
25. I. Osorio, M.G. Frei, D. Sornette, J. Milton, Y.C. Lai, Phys. Rev. E **82**, 021919 (2010)
26. R.B. Stothers, Science **224**, 1191 (1984)
27. N.I. Deligne, S.G. Coles, R.S.J. Sparks, J. Geophys. Res. **115**, B06203 (2010)
28. C.A. Chesner, W.I. Rose, A. Deino, R. Drake, J.A. Westgate, Geology **19**, 200 (1991)
29. M. Rampino, S. Self, Science **262**, 1955 (1993)
30. B.D. Malamud, G. Morein, D.L. Turcotte, Science **281**, 1840 (1998)
31. B.D. Malamud, J.D.A. Millington, G.L.W. Perry, Proc. Nation. Acad. Sci. USA **102**, 4694 (2005)
32. J.D.A. Millington, G.L.W. Perry, B.D. Malamud, Geol. Soc. London, Spec. Publ. **261**, 155 (2006)
33. T.J. Brown, B.L. Hall, C.R. Mohrle, H.J. Reinbold, CEFA Report 02-04 (2002)
34. R.A. Minnich, Science **219**, 1287 (1983)
35. R.A. Minnich, Conservation Biology **15**, 1549 (2001)
36. C.P. Weatherspoon, C.N. Skinner, Tech. rep., UC Davis, Centers for Water and Wildland Resources (1996), sierra Nevada Ecosystem Project: Final report to Congress, vol. II, Assessments and scientific basis for management options
37. A.H. Taylor, C.N. Skinner, Forest Ecol. Manag. **111**, 285 (1998)
38. J.K. Agee, C.N. Skinner, Forest Ecol. Manag. **211**, 83 (2005)
39. M.R. Yoder, D.L. Turcotte, J.B. Rundle, Phys. Rev. E **83** (2011)
40. B. Drossel, F. Schwabl, Phys. Rev. Lett. **69**, 1629 (1992)
41. S.F. Tebbens, S.M. Burroughs, Physica D **211**, 221 (2005)
42. B.D. Malamud, D.L. Turcotte, F. Guzzetti, P. Reichenbach, Earth Surf. Proc. Landforms **29**, 687 (2004)
43. P. Bak, C. Tang, K. Wiesenfeld, Phys. Rev. A **38**, 364 (1988)
44. D.R. Maidment, *Handbook of Hydrology* (McGraw-Hill, New York, 1993), ISBN: 0070397325
45. B.D. Malamud, D.L. Turcotte, C.C. Barton, Env. Eng. Geosc. **2**, 479 (1996)
46. B.D. Malamud, D.L. Turcotte, J. Hydrol. **322**, 168 (2006), hydrofractals '03
47. J.E. O'Connor, L.L. Ely, W.E. Wohl, L.E. Stevens, T.S. Melis, V.S. Kale, V.R. Baker, J. Geol. **102**, 1 (1994)